3D PROFILE DESIGN AND OPTIMIZATION OF A ROTOR FOR A LOW SPEED AXIAL COMPRESSOR WIND TUNNEL

Jan Mihalyovics, Julian Gambel, Dieter Peitsch,
Technische Universität Berlin,
Faculty V of Mechanical Engineering and Transport Systems,
Institute of Aeronautics and Astronautics,
Chair of Aero Engines,
Marchstr. 12, 10587 Berlin, Deutschland

Abstract

The chair of aero engines at the Technical University of Berlin operates a low speed compressor test rig used for experimental investigations on the influences of a pressure-gain combustion on compressor components. Current interests and major projects focused on the compressor stator. The wind tunnel shall be extended with a rotor to investigate the performance during periodic throttling invoked by pressure-gain combustion. To achieve the conception criteria a rotor was designed and subsequently optimized. This was done in a classic 2D approach utilizing the MISES collection of programs for cascade analysis and design. Amongst others, MISES was used for a systematical parameter study. Subsequently, objective functions were defined to select optimal profiles on each rotor blade design section. The blade design derived from the parameter study was then processed with the ANSYS CFD suite. Within the ANSYS workbench, a response surface based optimization was performed using a limited set of input parameters that define the blade geometry and a set of output parameters that quantify the calculated flow field.

Keywords

compressor blade optimization; CFD; low speed; axial compressor; aerodynamic design; wind tunnel

INTRODUCTION

The paper presents the 2D design of a rotor blade which is subsequently modified and optimized, resulting in a new 3D rotor blade geometry. The objective of the presented work is to perform numerical studies and an optimization on a compressor rotor to be designed and used in the low speed, open circuit wind tunnel at the Chair for Aero Engines at the TU Berlin. The wind tunnel is used for experimental investigations as part of the collaborative research center (*CRC*) 1029 [1]. Its main objective is the investigation on the influence of a pressure gain combustion (*PGC*) on compressor components. The wind tunnel design was chosen to create enhanced three-dimensional flow characteristics in an annular compressor stator and thus to enable investigations of the effects of a PGC at a high spatial resolution. In first attempts to study three-dimensional flow characteristics in the wind tunnel, variable inlet guide vanes (*VIGVs*) were used to provide the needed swirl for the stator cascade [2, 3]. For these experiments *VIGVs* were designed as three-dimensional blades by means of *RANS* simulations to ensure a baseline rotor like inlet profile on the stator cascade. For upcoming experiments with a newly developed cascade of 3D optimized stator blades [4], a suitable rotor is to be aerodynamically designed and optimized in terms of minimizing total pressure losses and extending the operating range. For this rotor, circumferential flow and pressure profiles were already specified by the existing *VIGV* design used in the earlier experiments and had to be met to accompany the already existing 3D optimized stator row. The present paper is structured as follows: at first a brief overview on the numerical setup used for the computational fluid dynamics (*CFD*) is presented, followed by a description of the 2D design process with a subsequent parameter study. Finally, the optimization is described in detail before concluding with the results.

In the area of the approximately two-dimensional main flow, turning and loss production are more or less predictable within narrow limits due to the extensive experience with axial compressor profile design found in the literature. However, these design criteria found in the literature do not – or only to a small part – apply for flows near the blade tips and the end walls. In consequence, both stability as well as efficiency can be influenced disproportionately by the end wall areas and the secondary flows to be found there.

Aerodynamic optimization techniques are divided into two main categories: gradient-free and gradient-based methods. Gradient-free approaches such as evolutionary algorithms are global optimizers finding a global optimum solution to a problem. However, they require a large number of function evaluations. The computational cost of

doi:10.25967/490163

these techniques scale with the number of design parameters, but can be mitigated using response surface approximations as demonstrated in [5, 6]. An efficient way to calculate the gradient information is using the adjoint method presented in [7, 8, 9, 4], thus providing the full gradient at a cost of solving a linear system. Unfortunately, this approach is still subject to research and currently not implemented in industrial applications. In gradient-based methods the optimization is driven by the gradient information to more efficiently minimize the problem's cost function. In CFD applications the gradient of the objective function with respect to the design parameters can be computed using finite-differences. This approach is available in most of the current engineering simulation and 3D design software packages providing *CFD* capabilities. An alternative approach for the optimization is not to perform the calculations for the entire blade at once but only sequentially at one blade section at the same time simulating the 3D flow around the entire blade. In the present publication, a two-stage design approach was chosen for reasons of time and available resources. First a 2D design with a subsequent parameter study on section level was performed. In a second step, the result was evaluated using CFD and a subsequent 3D optimization was carried out. The toolchain used for this two-stage design approach utilized only commercially available engineering simulation and 3D design software packages.

NUMERICAL SETUP

All numerical simulations were performed using a 3D *RANS* Solver (ANSYS CFX). The simulation type was steady state and fully turbulent (without transition modeling), employing the SST turbulence model with automatic wall functions. The compressible ideal gas fluid model was used to account for maximum Mach numbers of around 0.4 in the tip gap vortex. The computational domain comprised a single rotor blade passage and extended $0.4\,\mathrm{m}$ upstream and $0.2\,\mathrm{m}$ downstream (5 and 2.5 chord lengths, respectively) from the blade stacking line (see Figure 1).

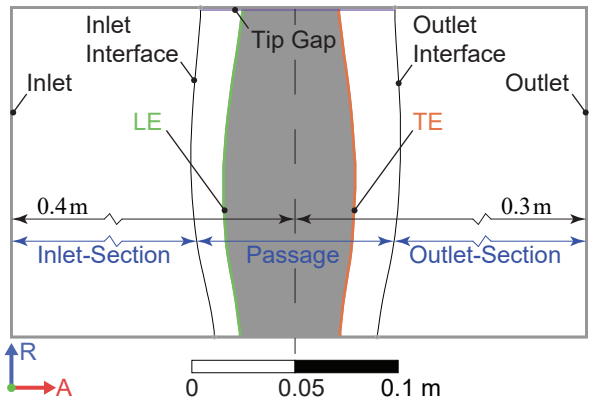

Fig. 1: COMPUTATIONAL DOMAIN USED FOR THE CFD CALCULATIONS

TurboGrid was used for automated, parametric generation of multi-block-structured hexahedral meshes. The mesh features three regions, the passage with an O-H-block structure around the blade as well as inflow and outflow H-block up- and downstream of the passage (see Figure 2). Among other parameters, the mesh density is mainly determined using the *global mesh size factor*, which controls the number of elements in the blade-to-blade plane, the number of elements along the blade span and in the tip gap, as well as the first element offset and the wall-normal expansion ratio, which together determine the number of elements in the blade surface boundary layer. The entire domain was set to rotating.

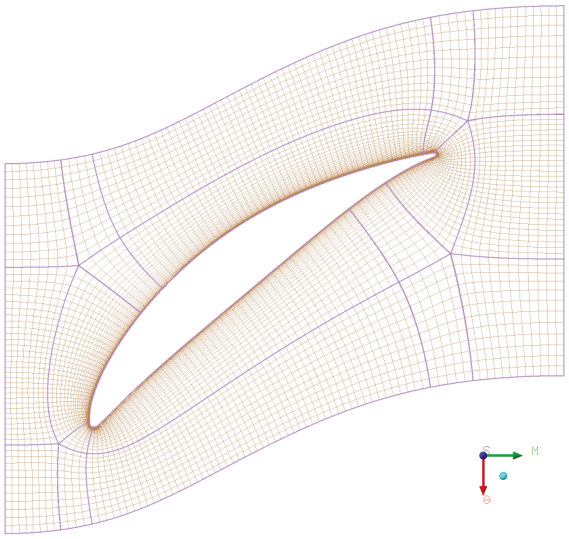

Fig. 2: EXAMPLARY TURBOGRID PASSAGE MESH AT THE HUB-SECTION

The casing wall and the hub segments in the inflow and outflow regions were set to counter-rotating. Total pressure ($101325\,\mathrm{Pa}$), total temperature ($293\,\mathrm{K}$) and flow turbulence ($5\,\%$) were specified at the inlet, while the mass flow rate, which determined the operating point, was specified at the outlet. To evaluate the compressor performance, evaluation planes were defined at $0.2\,\mathrm{m}$ upstream and $0.1\,\mathrm{m}$ downstream of the stacking line. In a mesh sensitivity study, the influence of the aforementioned parameters on total pressure rise, loss coefficient and flow stability at an operating point near stall were investigated. While the effect of span-wise and boundary layer resolution was small enough to retain or even reduce the number of nodes in these directions, the influence of the global mesh size factor was significant and convergence could not be achieved in the investigated range. Particularly, a higher mesh size factor was shown to delay the onset of stall at the rotor tip, as cases with reduced mesh size factor exhibited severe flow separation while those with a higher factor did not. To keep the number of mesh elements and computation time within reasonable limits for the optimization, the mesh size factor could only be moderately increased. It was also found that the position and shape of the region interfaces between the passage and the inflow and outflow regions (i.e. their distance from the leading edge (*LE*) and trailing edge (*TE*) of the blade at different radial sections) affected the number of mesh elements on the blade-to-

blade surface and thereby also affected total pressure rise, loss coefficient and flow stability. Unfortunately, the correlation between interface position and number of elements was unpredictable for different blade shapes, inducing additional uncertainty.

2D MISES DESIGN

The outflow conditions for the rotor to be designed are predefined by the *VIGV* set used in earlier experiments and these are depicted in Figures 3 and 4. The design objectives of the baseline rotor were chosen to convert a shaft power of $24.5\,\mathrm{kW}$ at a speed of $3500\,{}^{1}/_{\mathrm{min}}$ assuming a design mass flow of $9.5\,{}^{\mathrm{kg}}/_{\mathrm{s}}$ (resulting from an assumed density of $1.2\,{}^{\mathrm{kg}}/_{\mathrm{m}^3}$ and a constant flow velocity of $38\,{}^{\mathrm{m}}/_{\mathrm{s}}$ at an inlet total pressure of $101325\,\mathrm{Pa}$).

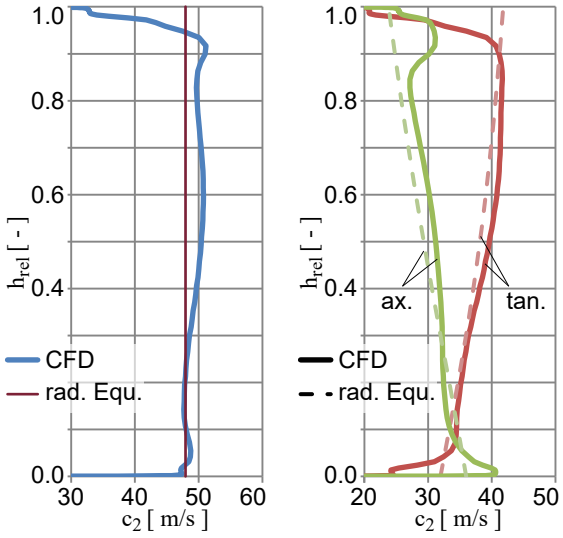

(a) velocity (b) axial and tangential velocity

Fig. 3: PREDEFINED OUTFLOW VELOCITIES AT DESIGN POINT IN THE ABSOLUTE SYSTEM

This accounts for a specific work of $\Delta w_s = 2928\,{}^{\mathrm{J}}/_{\mathrm{kg}}$. The blades of the baseline rotor are designed for a constant displacement of work over the blade height. It is desired to achieve a broad operating range, as the rotor is to be used for experiments at periodically-transient boundary conditions. The essential performance values of the rotor are already determined by the predefined outflow velocity and outflow angle profiles. However, there is some freedom of design with regard to important dimensioning parameters such as number of blades, chord length or axial overall length of the rotor, as well as the profile shape of the blades including related parameters such as camber, maximum camber, thickness and maximum thickness as well as *LE* and *TE* radius. The number of blades has been set to $n_{base} = 19$ which is the number of *VIGVs* used in the earlier experiments. In a first step, a simplified analytical quasi-3D design of the rotor blades was caried out. The variation of the velocity triangles over the blades spanwise direction, i.e. the turning in the relative system, is determined taking into account the radial equilibrium additionally considering the approach of exponential blading. Subsequently, suitable blade profiles (NACA65) are selected on several design sections (Figure 5a) in order to achieve the respective flow turning.

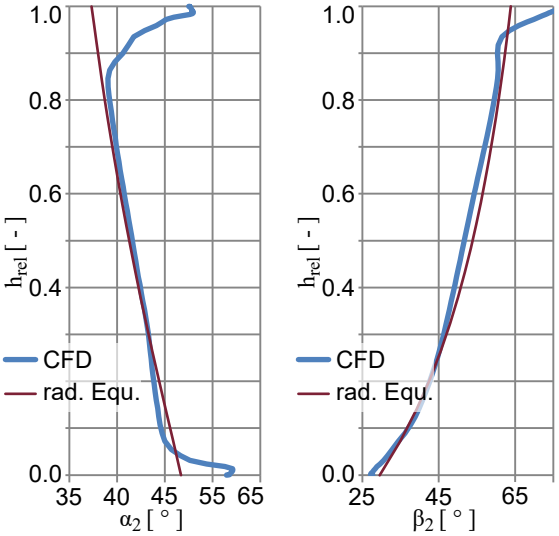

(a) Absolute outflow angle (b) Relative outflow angle

Fig. 4: PREDEFINED OUTFLOW ANGLES AT DESIGN POINT

Observing that the flow velocity in the absolute system behind the rotor in span wise direction is almost constant, provides an initial solution statement for the radial equilibrium:

$$c_2 = \text{const.} \neq \mathrm{f}(r) \tag{1}$$

The inflow condition is considered axial ($c_{u1}(r) \equiv 0$), thus the distribution of work in the rotor depends only on the outflow condition. All terms in equation 3.2 (see [10]) can be expressed by the constant c_2 and the unknown function $\alpha_2(r)$:

$$c_2 \frac{dc_2}{dr} = 0 \tag{2}$$

$$\frac{c_{u2}^2}{r} = c_2^2 \frac{\sin^2(\alpha_2(r))}{r} \tag{3}$$

$$\frac{dh_t}{dr} = \frac{d(u_2 c_{u2} - u_1 c_{u1})}{dr} = \frac{d(\Omega r c_2 \sin(\alpha_2(r))}{dr} \tag{4}$$

$$= \Omega c_2 \frac{d(r \sin(\alpha_2(r)))}{dr} \tag{5}$$

Equation 5 becomes a nonlinear differential equation for $\alpha_2(r)$:

$$\Omega c_2 \frac{d(r \sin(\alpha_2(r)))}{dr} = c_2^2 \frac{\sin^2(\alpha_2(r))}{r} \tag{6}$$

This equation can be integrated between the Euler radius and any radius using the substitution $S(r) = r \sin(\alpha_2(r))$. The result for the function $\alpha_2(r)$ is:

$$\alpha_2(r) = \sin^{-1}\left(\frac{1}{\frac{c_2}{2\Omega r}\left(1 - \frac{r^2}{r_E^2}\right) + \frac{r}{r_E}\frac{1}{\sin(\alpha_2(r_E))}} \right) \tag{7}$$

The flow angle at the Euler radius is interpolated from the given flow angle profile of the baseline rotor. Assuming a

constant density, the velocity c_2 is determined by integrating the mass flow from hub to the tip.

$$\dot{m} = \int_{r_i}^{r_a} \rho c_2 \cos\alpha_2 dA \tag{8}$$

$$= 2\pi\rho c_2 \int_{r_i}^{r_a} \cos(\alpha_2(r)) r dr \tag{9}$$

After converting to c_2, inserting the expression for $\alpha_2(r)$ and using the identity $\cos(\sin^{-1} x) = \sqrt{(1-x^2)}$ one may derive:

$$c_2 = \frac{\dot{m}}{2\pi\rho} \frac{1}{\int_{r_i}^{r_a} \sqrt{1 - \left(\frac{1}{\frac{c_2}{2\Omega r}\left(1 - \frac{r^2}{r_E^2}\right) + \frac{r}{r_E}\frac{1}{\sin(\alpha_2(r_E))}} \right)^2} r dr}$$

Since the unknown c_2 is contained in the integral term, the equation must be solved iteratively. The value from a previous iteration can be used to evaluate the integral, which is done numerically using a suitable programming language. A comparison of the analytical solution for the radial equilibrium with the corresponding *CFD* calculation shows a good agreement for the outflow angle $\alpha_2(r)$ in the range of about $35\,\%$ to $85\,\%$ of the blade height. It can be seen in the analytical solution that the flow angle is somewhat steeper (Figure 4a). The flow angle near the side walls for the baseline rotor, especially at the tip side is increasing sharply. This is due to the reduced flow velocity in the boundary layers visible in Figure 3b and the resulting over turning at the blade tip, also caused due to the influence of the tip gap vortex. To define the blade geometry, the annulus is divided into 20 equal-area segments. There are 21 radial positions as boundaries of these segments, the first of which coincides with the hub, the last with the casing (Tip). This is shown in Figure 5a.

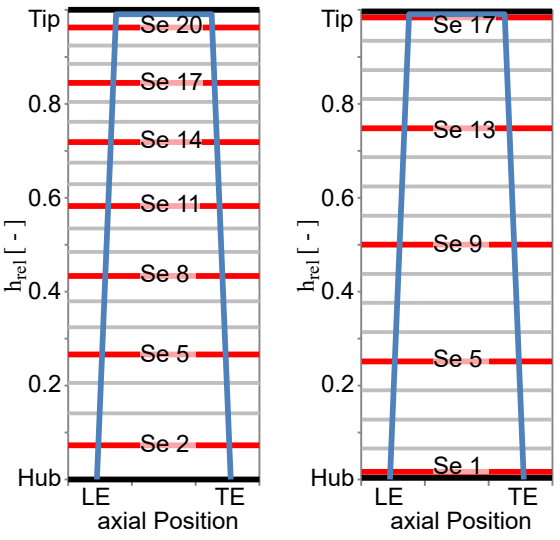

(a) 2D MISES (b) Optimization

Fig. 5: CORESPONDING DESIGN SECTIONS FOR THE 2D MISES DESIGN AND THE SUBSEQUENT OPTIMIZATION

The profiles are designed for seven of the 21 sections. These are, sections 2, 5, 8, 11, 14, 17 and 20 (marked in red in Figure 5a). The hub and tip sections are deliberately omitted as they are located in the respective boundary layers. The profiles on the remaining sections are created in a subsequent step by interpolating the profile parameters. The proven NACA65 family of profiles is used for the preliminary design. Having been extensively researched theoretically, experimentally and numerically, this profile family provides reliable design criteria and comparative data which can be found in the literature. Choosing NACA65 profiles to be used, already determines a number of profile parameters: the maximum camber is $50\,\%$, the maximum thickness is $37.5\,\%$. Furthermore, the leading edge radius depends on the relative thickness expressed as percent of the chord. A value of $0.6\,\%$ of the chord length is selected for the *TE* radius. Since the original profile contour of the NACA65 series has a sharp *TE* with zero thickness, a $(1-\cos(c_{mod}))$-shaped blending function is applied to the rear $40\,\%$ of the skeleton line providing a smooth transition. Aungier [11] presents formulas for optimal profile camber and staggering of NACA65 profiles to fulfill the turning task of β_1 to β_2 with the lowest possible losses depending on the relative pitch and the relative profile thickness. These formulas are based on empirical measurement data for linear compressor cascades where the axial flow velocity at the inlet and outlet is usually kept constant by means of boundary layer suction. In the present case, the condition of a constant axial velocity according to the radial equilibrium does not apply to all blade sections considered. At the hub, the flow is decelerated in the axial direction, causing additional diffusion and thus aerodynamic load, while the flow is accelerated at the tip section. To take this into account, Grieb [12] corrects the inflow and outflow angles for which the profiles are designed on the various blade sections. The vectors of the relative velocities upstream and downstream of the blade are modified in such a way that the axial components of the inflow and outflow are both set to the mean value $c^*_{ax,1} = c^*_{ax,2} = c_{\mathrm{inf},ax} = \frac{c_{ax,1}+c_{ax,2}}{2}$, while the circumferential components are kept constant. The resulting flow angles β^*_1 and β^*_2 correspond to a larger ($c_{ax,1} > c_{ax,2}$) or smaller ($c_{ax,1} < c_{ax,2}$) effective turning for a linear cascade. The camber must be increased or decreased accordingly.

Parameter study using MISES

The relative pitch or chord length as well as the relative thickness of the profiles are not yet defined and optimal values must be found. A parameter study regarding chord length and relative thickness on seven blade sections was conducted using the MISES set of programs for cascade analysis and design. The chord length was varied between $60\,\mathrm{mm}$ and $110\,\mathrm{mm}$ in steps of $5\,\mathrm{mm}$ (11 values), the relative thickness between $5\,\%$ and $11\,\%$ in steps of $1\,\%$ (7 values). The relative pitch, inversely proportional to the chord length, depends on the radial position of the blade section under consideration and increases towards the outside with the same chord length. For each section, 77 profile variants are calculated, resulting in a total of 539 profiles. The profile coordinates in the dimensionless (m', θ) coordinate system are calculated with a scripting language and saved

as text files formatted as input for MISES. To determine the operating range for cascaded profiles, MISES has the ability to calculate loss loops using a parameter sweep over a user-defined inflow angle range. This feature uses the converged solution for an inlet angle as the starting solution for the next larger or smaller angle, achieving rapid convergence. For a rotor, the inflow angle changes to varying degrees with changes in the mass flow in span wise blade direction. This is significant for hub sided flows. However, the aerodynamic load (deceleration) at the blade tip changes even more. The angle of inflow range examined on the various sections with MISES is selected in order to correspond exactly to the change in the axial velocity at the inflow plane, caused by a change in the inflow angle of $\pm 5^\circ$ on section 2. Starting from the design point, eight angle intervals up to the largest and smallest inflow angle are evaluated for each positive and negative incidence. The actual number of calculated inflow angles for each curve can deviate from this due to interval division and/or premature termination of the loss loop. To classify the results, it is helpful to compare the loss and deviation angle[1] loops for the profile variants. Qualitative depictions of the parameter study are shown in Figure 6 and Figure 7 as examples for sections 5. For a better overview only a part of the variants of the parameter study are shown; the chord lengths 65 , 75 , 85 , 95 and $105\,\mathrm{mm}$ as well as the relative thicknesses 6 , 8 and $10\,\%$ have been omitted.

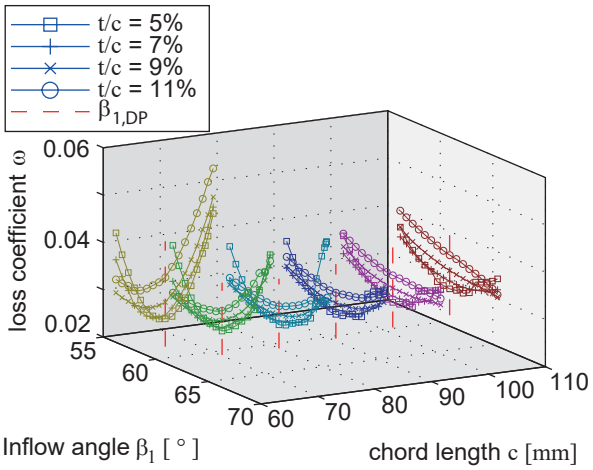

Fig. 6: LOSS LOOPS (ω vs. β_1) FOR CHORD LENGTH $c = 60 \cdots 100\,\mathrm{mm}$ OF SECTION 5

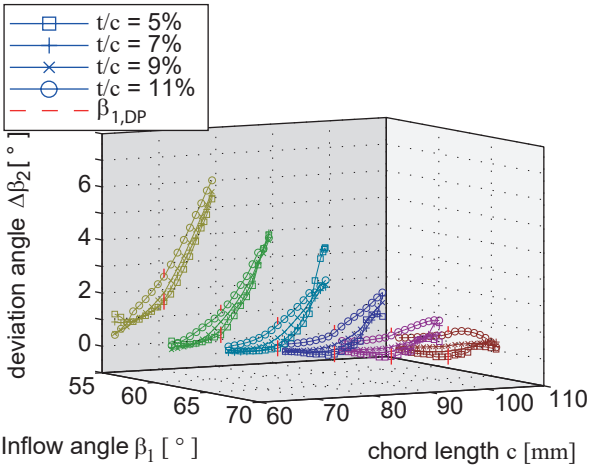

Fig. 7: DEVIATION LOOPS ($\Delta\beta_2$ vs.β_1) FOR CHORD LENGTH $c = 60 \cdots 100\,\mathrm{mm}$ OF SECTION 5

At first glance, the parameter study confirms the relationships to be expected: thinner profiles have a lower loss coefficient at the design point, but this increases with a change of the inflow angle. The greater the chord length of the profiles, the less the loss coefficient increases and the less the outflow angle changes with changes of the inflow angle. With regard to the blade turning at the design point, it should be noted that the design method used by Aungier did not deliver satisfactory results with respect to the outflow angle profile presented in Figure 4a. It was expected that the determined outflow angle using the radial equilibrium should actually be calculated for all profile variants in the design point. In section 5, the outflow angle decreases with thinner and elongated profiles, but this does not apply in general to the other sections. There is an inverse correlation between the outflow angle and the static pressure ratio. On closer inspection, however, some of the loss loops reveal inconsistencies that raise questions concerning the calculation method with respect to the operating range of the blade profiles. In some cases, the loss coefficient increases sharply at a few degrees of both positive and negative incidence, and then increases moderately as the incidence continues to increase. This is accompanied by a slight offset in the outflow angle curve. This effect mainly occurs with very thin profiles ($t/c = 5 \cdots 7\,\%$) and may be explained by the formation of a separation bubble with a turbulent reattachment of the boundary layer. In some cases, however, both the calculated loss coefficient and the calculated outflow angle decreases with increasing positive incidence. This occurs mainly with thick profiles, but occasionally also with thinner profiles. The explanation for this is an algorithm in the solver of MISES for cases of a detached boundary layer with its location of separation oscillating over the iterations. In order to force numerical convergence, the boundary layer (or its separation point) is fixed at one location.

In consequence the loss coefficient and the flow angle are to small – both depending on the calculated boundary layer thickness in MISES. Since such results are not physically valid, while evaluating the curve data, it is determined for each curve whether the flow angle decreases at any point on the positive incidence branch. If this is the case, the corresponding results are marked as not valid. For the selection of optimal profiles on each section, objective, quantifiable criteria must be defined. Although an evaluation of the entire loss loop would be desirable, it is impracticable or not consistently possible due to the problems de-

[1] Here, the deviation angle refers to the calculated downstream flow angle minus the downstream flow angle as being achieved according to the radial equilibrium.

scribed above. Instead, an easily quantifiable variable was used. A combined loss coefficient (equation 10) was used for the selection of optimal values of chord length and relative thickness, which includes the loss coefficients at the design point as well as at the largest positive and negative incidence - provided with weighting factors of 3, 2 or 1.

$$\omega_{comb} = \frac{1}{6}\left(\omega_{CH} + 3 \cdot \omega_{DP} + 2 \cdot \omega_{ST}\right) \qquad (10)$$

The choice of the weighting factors is arbitrary, but results from the following consideration: The throttled/stalled operating condition is more critical in terms of compressor stability (and it is more difficult to extend the operating range in this direction) than the de-throttled operating condition and is therefore weighted twice as much.

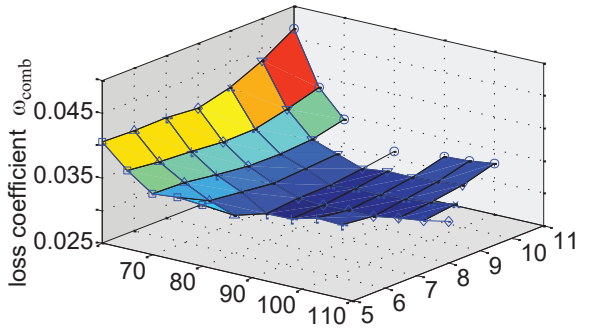

Fig. 8: WEIGHTED LOSS COEFFICIENT ω_{comb} VS. CHORD LENGTH AND REALTIVE THICKNESS FOR SECTION 5

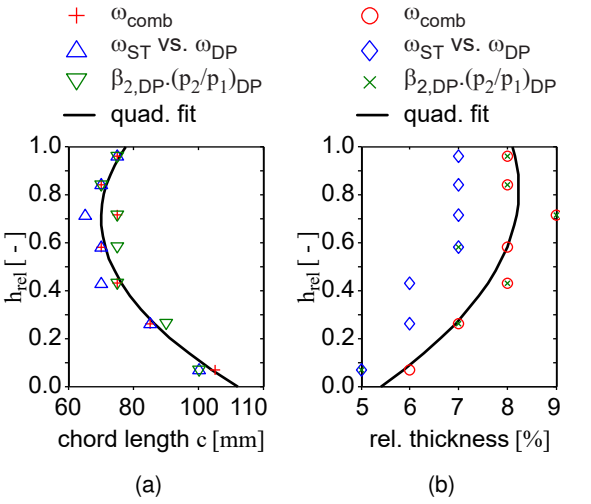

Fig. 9: OPTIMAL VALUES FOR CHORD LENGTH AND RELATIVE THICKNESS FOR VARIOUS CRITERIA, INTERPOLATION FOR ω_{comb}

The design point, however, is the most important condition for operation and is therefore weighted as much as the other two operating points together. Figure 8 shows the combined loss coefficient for the parameter space on section 5. Figure 9 shows the optimal values for chord length (9a) and relative thickness (9b) selected according to various criteria for the seven sections considered in the parameter study. For the definition of all 21 sections of the three dimensional blade, the optimal values determined according to the combined loss coefficient are interpolated by 2nd order polynomials, which smooth the somewhat jagged data. Subsequently, blade profiles are designed with the values for chord length and relative thickness calculated on all 21 sections according to the method described above and stacked radially over one another in their respective center of gravity. The comparison of the outflow profiles with the baseline design and the result of the parameter shows, that the systematically derived blade design using the parameter study does not completely fulfill the desired turning. In the absolute system the outflow angle is lower almost over the entire blades spanwise direction when compared to the baseline design. Only at the lower $20\,\%$ of the blade height, where the initial design had a corner separation, the turning of the new design shows improvements (see Figure 10). In the relative system, the comparison with the radial equilibrium solution used to define the turning task for the blade profiles shows that it was exceeded at the blade tips but missed at the blade's center section. Accordingly, the total pressure and the static pressure ratios are lower at the design point. The efficiency and loss coefficient, on the other hand, are better when compared with the initial design. Table 1 presents a comparison of the 2D MISES design with the baseline design. As depicted in Figure 14 the silhouette of the resulting rotor blade (2D MISES design) differs from the baseline design.

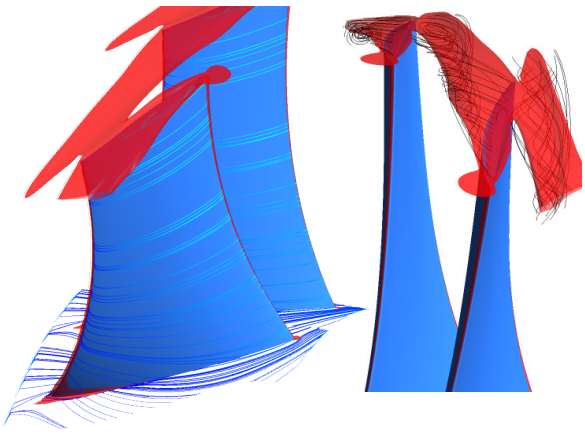

(a) Suction Side (b) Blade Tip

Fig. 10: SECONDARY FLOWS OF THE SYSTEMATICALLY DESIGNED MISES BLADE AT DESIGN POINT

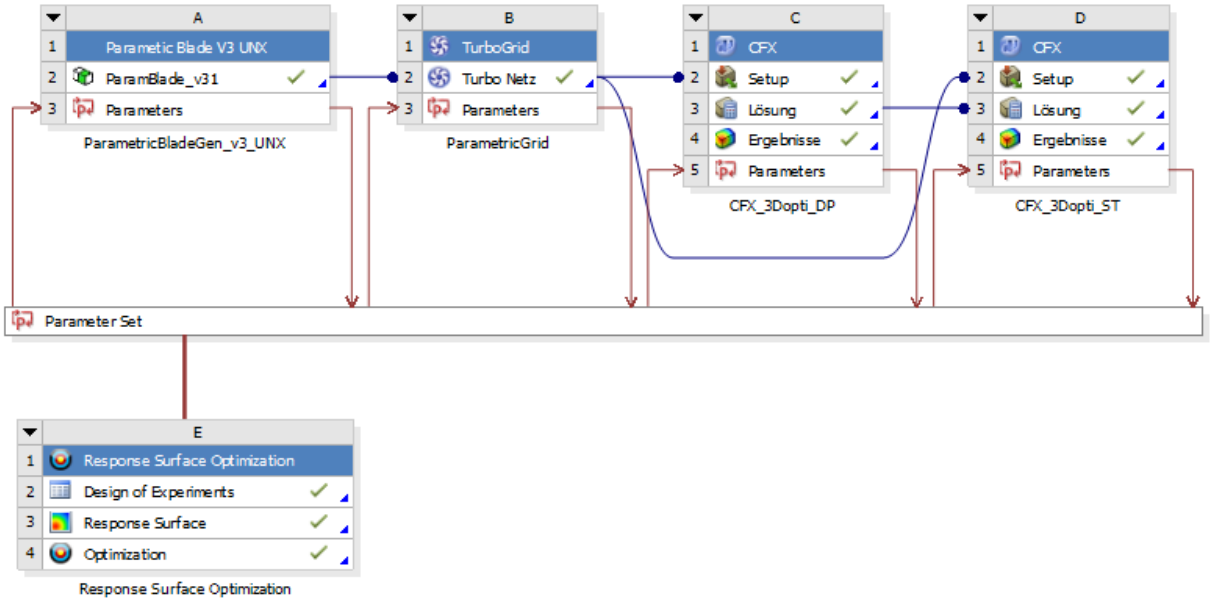

Fig. 11: PROJECT SCHEME OF THE OPTIMIZATION IN THE ANSYS WORKBENCH

Tab. 1: COMPARISON OF THE BASELINE DESIGN AND THE SYSTEMATICALLY DESIGNED MISES BLADE

Name	baseline	2D MISES
DESIGN POINT (DP)	$9.5\,\mathrm{kg/s}$	$9.5\,\mathrm{kg/s}$
total pressure	$2865.0\,\mathrm{Pa}$	$2712.5\,\mathrm{Pa}$
static pressure ratio	1.02223	1.02137
isentropic efficiency	93.02%	93.18%
loss coefficient	0.03016	0.02638
HIGHEST p_t	$8.4\,\mathrm{kg/s}$	$8.5\,\mathrm{kg/s}$
total pressure	$3263.7\,\mathrm{Pa}$	$3082.8\,\mathrm{Pa}$
static pressure ratio	1.02441	1.02315
isentropic efficiency	92.89%	93.26%
loss coefficient	0.03117	0.03045
CHOKED DP	$11.416\,\mathrm{kg/s}$	$11.416\,\mathrm{kg/s}$
total pressure	$1974.6\,\mathrm{Pa}$	$1976.2\,\mathrm{Pa}$
static pressure ratio	1.01612	1.01616
isentropic efficiency	90.61%	90.69%
loss coefficient	0.04316	0.04249

OPTIMIZATION

Since the systematically designed blade was not able to satisfactorily fulfill the turning task and the performance fell behind the original design when throttled, various changes to the blade design were realized, as described in the following. The profiles on hub and tip were retained. In between the hub and tip sections the chord length was linearly interpolated (thus increased compared to the 2D MISES design), while the relative thickness as well as the camber angle and stagger angle of the 2D MISES design profiles were retained. The increased chord length reduced the relative pitch, reducing the incidence and the turning angle. In consequence the blade turning improved. Since the improvement of the turning at the blade center did not result in the desired outflow profile of the initial baseline design, the approach of designing the profiles according to the solution of radial equilibrium was rejected. Instead, target values for the exit angles from the profiles were defined directly using the exit profile ($\beta_2(r)$) from the original baseline simulation (see Figure 4b). Its values between $15\,\%$ and $80\,\%$ of the blade height were supplemented with the angle from the solution for the radial equilibrium at the casing. For the first blade designed on the basis of this modified β_2 profile, the chord length was increased in the center and at the tip of the blade when compared to the 2D MISES design, while the length at the hub was slightly shortened. The basic characteristic of the silhouette, a constriction in the chord length at about $70\,\%$ blade height, was retained. For the profile thickness, a constant value of $6\,\mathrm{mm}$ was specified over the entire blade height, which corresponded to the values for the 2D MISES design. As a result, the relative thickness of the blade tip decreased compared to the 2D MISES design. With this design, the turning task of the baseline rotor design was (over)-fulfilled for the first time over the entire blade height. At the design point and with increased mass flow, the new design consistently showed better performance paramet-

ers than the baseline design. Even at throttled design points, the new design initially performed well and achieved higher maximum values for the total pressure, the static pressure ratio and the efficiency. In a final design modification, the number of blades was reduced from 19 to 13, at the same time the chord length was multiplied by the factor 19/13, so that the relative pitch remained constant. Reducing the number of blades caused a significant expansion of the operating range of the rotor in combination with a corresponding enlargement of the chord length keeping a constant relative pitch and relative profile thickness. The relative thickness and construction angles of the profiles were also retained resulting in a so-called Wide Chord Blade. This improvement is primarily due to the reduction of the relative gap dimension at the blade tip, which, in addition to the expansion of the operating range, has also led to a reduction in tip vortex losses. The resulting blade serves as the basis for the subsequent algorithm-based optimization procedure. A further reduction in the number of blades with correspondingly larger blades was not considered with regard to the blade mass (centrifugal forces in the blade-hub connection) and the axial overall length of the rotor.

For the optimization procedure using the ANSYS CFD-Suite, the blade geometry must be defined using a limited number of parameters. The maximum number of input parameters that can be simultaneously changed during a response surface-based optimization in the ANSYS Workbench is limited to 12 or 20, depending on the algorithm used for the Design of Experiment (*DoE*). The investigation of different variants during the preliminary 2D MISES design of the blade showed that the operating range of the rotor – being limited during throttling events by flow separation at the housing or at the tip of the blades – is significantly influenced by the chord length in the mid blade height. In this respect, a configuration was found which has a better operating range with lower losses than the initial baseline design. However, the preliminary investigation did not clarify how the operating range can be extended as efficiently as possible when changing the distribution of the chord length over the blade height. Thus, it seems reasonable to include the chord length on several sections simultaneously in the 3D algorithm-based optimization procedure. In order to remain within the scope of a maximum of 20 parameters, compromises must be made with regard to the number of sections to be optimized (see Figure 5b) and the number of parameters per section. For the parametric definition of the blade geometry, five sections at $0\,\%$, $25\,\%$, $50\,\%$, $75\,\%$ and $100\,\%$ of the blade height are used. On each of these sections the primary parameter is the chord length c, the profiles being used are modified NACA65 profiles, whose base values for camber angle and stagger angle are designed with the algorithm already used in the preliminary design.

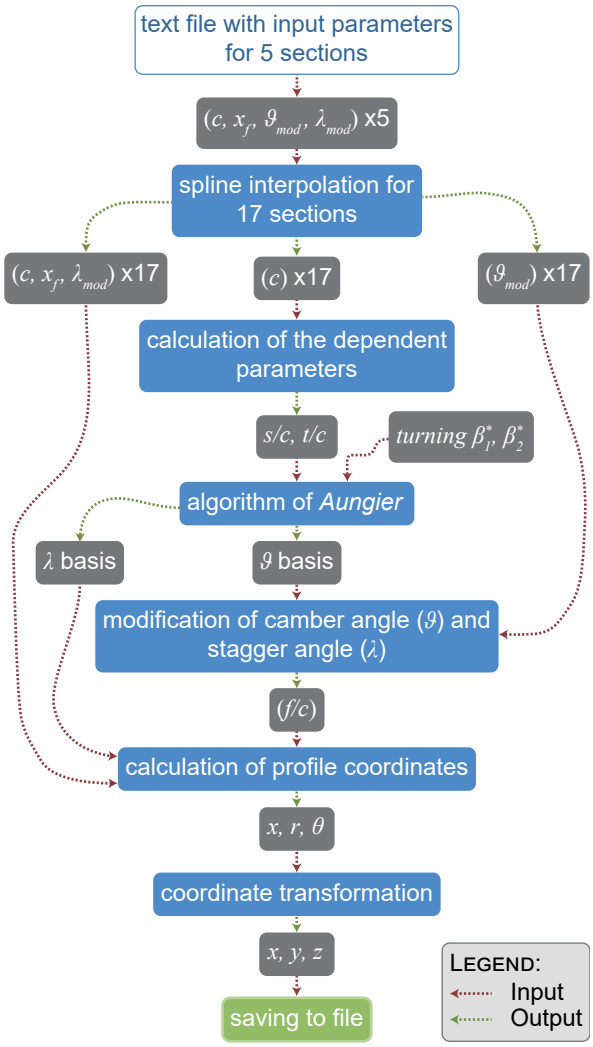

Fig. 12: SCHEMATIC FLOWCHART OF THE BLADE GENERATING TOOL

As additional design parameters the maximum camber x_f, which allows the diffusion in the blade passage to be adjusted, and modifications for the camber angle (ϑ_{mod}) and stagger angle (λ_{mod}), which in combination allow the incidence to be fine-tuned to the profiles and the flow angle of the blade are being used. The number of blades is kept constant at 13. As it was the case with the baseline design, the thickness of the profiles is fixed, it is linear between $19/13 \cdot 7.5\,\mathrm{mm} \approx 10.96\,\mathrm{mm}$ at the root of the blade and $19/13 \cdot 6.0\,\mathrm{mm} \approx 8.77\,\mathrm{mm}$ at the tip of the blade. Due to limitations of the Blade Editor tool provided by the ANSYS Suite, a script was written for a customizable geometry creation (see Figure 12). Using the input parameters, this script calculated the profile coordinates for a total of 17 blade sections (the five defining sections at $0\,\%$, $25\,\%$, $50\,\%$, $75\,\%$ and $100\,\%$ channel height as well as a total of twelve evenly distributed sections in between). After calculating the profile coordinates, the script saved these in a text file in the same format as it would be generated by the ANSYS DesignModeler, so that it could be used by the blade meshing tool TurboGrid. The script was compiled to a standalone executable binary and subsequently integ-

rated into the work flow of the simulation within the ANSYS Workbench using an External Connection Module. As a result the entire work flow for the optimization could be implemented as an ANSYS Workbench project as depicted in Figure 11. The work flow for each design point (i.e. a set of geometry parameters) consists of geometry creation (A), cross-linking of the calculation area with TurboGrid (B) and the CFD simulation with CFX for two flow cases. These are: the design point (C) and a throttled operating point (D). The mass flow at the throttled operating point was chosen conservatively to be $8.4552\,\mathrm{kg/s}$, i.e. within the expected operating range of all designs. The reason for this being, that a stall at individual design points would lead to strong fluctuations in the response surfaces and reduce their predictive power. However, an additional fundamental dilemma of the response surface-based optimization is that the *DoE*s do not simulate the interesting operating range outside the capabilities of the original baseline design. As the de-throttled operating condition is not critical for a subsonic compressor the addition of a simulation thereof was omitted with in order to reduce the computing time. The settings in TurboGrid (grid parameters) and in the preprocessor, solver and postprocessor correspond to those discussed in the numerical setup (see section). In order to be able to adapt the downstream angle profile to the target (baseline rotor) profile during optimization, output parameters for the downstream angle in the absolute system at $10\,\%$, $20\,\%$, $30\,\%$, $40\,\%$, $50\,\%$, $60\,\%$, $70\,\%$, $80\,\%$ and $90\,\%$ spanwise blade height were added in the post-processor for the design point.

Before the Design of Experiments was created, the boundary values for all 20 input parameters were defined to reasonable limits. These are based on the values of the 2D MISES design and the conducted parameter study. These preliminary studies had shown that front loading of the profile has a positive effect on the losses and turning of the highly loaded profile. Thus, the permissible value range for the maximum camber on the housing was set to $0.35 \cdots 0.65$, i.e. in the direction of aft loading. Here it seems conceivable that a relief of the front blade area could reduce the tip gap flow. The values of the 2D MISES optimized design and the limits set for the *DoE* are summarized in Table 2. Optimal Space Filling was selected as the *DoE* type, the number of samples ("Sampling Type") was selected on the basis of the Central Composite Design. This resulted in 553 design points for the 20 input parameters. The response surfaces were calculated using the genetic aggregation algorithm. The computing time was several hours, which is negligible compared to the solver computing time of the 553 *DoE* design points. The response surfaces have been used to determine the dependence of the output parameters on the input parameters. It is difficult to display these response surfaces as a whole, since they are 20-dimensional according to the number of input parameters. They are therefore not presented here. It can be summarized that the compressor efficiency at design point is very little dependent on the input parameters, only the stagger angle modification λ_{mod}, especially at 75% blade height, has a significant influence. At the throttled operating point, the compressor efficiency correlates positively with the chord lengths at $0\,\%$, $25\,\%$, $75\,\%$ and $100\,\%$ blade height. Increasing the chord length at $75\,\%$ and $100\,\%$ has an increasing effect on the efficiency. At $50\,\%$ blade height the efficiency decreases with increasing chord length. Subsequently, the results of the response surfaces were used to find optimal design candidates. The optimization task at hand is a Pareto optimization, i.e. the optimization of a problem with multiple objectives. From the methods available in the ANSYS DesignXplorer, the Multi-Objective Genetic Algorithm (MOGA) was used for this task, which is a variant of the Non-dominated Sorted Genetic Algorithm-II (NSGA-II). A total of 15 optimization objectives are specified. The total pressure ratio, the static pressure ratio and the rotor efficiency at design point and at the throttled operating point are to be maximized. For the outflow angles α_2 at $10\,\%$, $20\,\%$, $30\,\%$, $40\,\%$, $50\,\%$, $60\,\%$, $70\,\%$, $80\,\%$ and $90\,\%$ blade height, target values are only given for the design point (taken from the outflow angle profile of the baseline design; see Figure 4). The geometry parameters of the design candidates, especially those of the most promising candidate, are not near the limits of the given value range presented in Table 2. It is therefore assumed that this has been chosen large enough to include the optimum. The most promising design candidate as well as the initial baseline were recalculated on a fine grid for more precise analysis and final evaluation. Figure 13 shows the chosen design candidate from the optimization result in comparison to the baseline rotor.

Tab. 2: BOUNDARY VALUES OF THE GEOMETRY PARAMETERS IN THE DoE

$h_{rel}\,[-]$		**0**	**0.25**	**0.5**	**0.75**	**1**
	-Lim	0.12500	0.12077	0.10751	0.10673	0.13036
$c\,[m]$	Base	0.14953	0.13419	0.11946	0.11859	0.14485
	+Lim	0.15000	0.14761	0.13140	0.13045	0.15933
	-Lim	0.3	0.35	0.35	0.35	0.35
$x_f\,[-]$	Base	0.5	0.5	0.5	0.5	0.5
	+Lim	0.5	0.55	0.55	0.55	0.65
	-Lim	-2	-2	-2	-2	-2
$\vartheta_{mod}\,[°]$	Base	0	0	0	0	0
	+Lim	2	2	2	2	2
	-Lim	-2	-2	-2	-2	-2
$\lambda_{mod}\,[°]$	Base	0	0	0	0	0
	+Lim	2	2	2	2	2

CONCLUSION

The resulting rotor design from the optimization (see Figure 14 (d)) shows a substantial increase in static and total pressure with a considerably higher mass flow range. In terms of efficiency and loss coefficient, the optimized blades are also showing a significant improvement. The optimized design candidate has a larger operating range than the baseline, achieving the largest total pressure build-up ($3573\,\mathrm{Pa}$) at a mass flow of $8.0\,\mathrm{kg/s}$. Due to its superior

operating range and the best mapping of the outflow angle profile at design point, the optimized rotor blade is selected as the blade design to be manufactured and will be used in the wind tunnel.

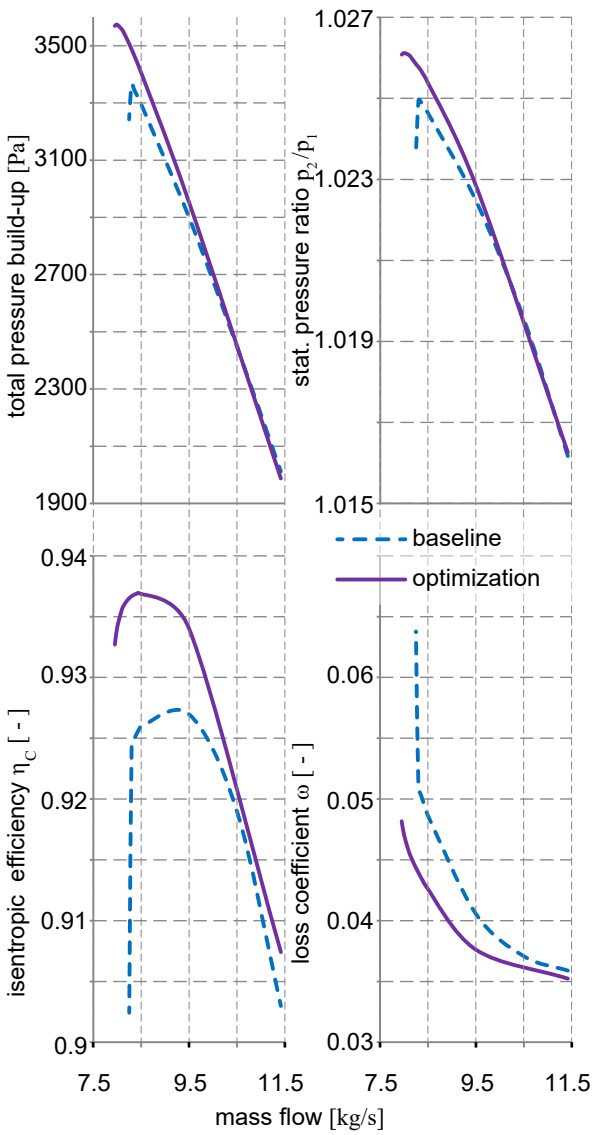

Fig. 13: COMPARISON OF THE OPTIMIZED ROTOR WITH THE BASELINE ROTOR

In the context of the present work, an axial compressor rotor was systematically designed using an analytical solution for the radial equilibrium, taking into account the outflow angle profile to be mapped. Subsequently, a parameter study was carried out for several blade sections with regard to chord length and profile thickness using MISES in order to select the most efficient profiles from the NACA65 family. As a result, the blade design was revised several times in an iterative process. The turning task for the profiles was redefined to achieve the desired outflow angle profile. In addition, the chord length in the blade center and at the blade tip was increased so that the performance values (operating range, turning and total pressure ratio) of the baseline design could be exceeded with lowering the losses. A significant improvement in the operating range was achieved by a wide-chord variant of the rotor design, in which the number of blades was reduced from 19 to 13 while at the same time the blade profiles were increased proportionally, so that the relative pitch remained constant. Furthermore, a response surface based pareto optimization of the 3D rotor blade using the ANSYS Workbench and the ANSYS DesignXplorer was performed. For this purpose a parametric blade model was created and implemented in an independent program, which was integrated into the workbench. In order to be able to change the entire blade geometry in a *DoE* during the optimization regarding secondary flow effects, the number of geometric parameters had to be limited to 20. This required compromises in the number of defining blade sections and the design freedom per section. Thus, four profile parameters: chord length, camber, maximum camber and stagger angle were varied on five blade sections. The resulting rotor design from the optimization met the required outflow angle profile in a satisfactory manner while being superior to the baseline design in terms of operating range and losses. Concluding the work, it can be summarized, that the operating range of the rotor at the turning task to be fulfilled is essentially limited by the interaction between the peak gap flow and the housing boundary layer. This is a highly non-linear problem in the sense of the interrelationships between geometry and flow field and their complex dependencies on the geometry parameters. For such problems, response surface based methods are basically only of limited use, so that another (gradient based) optimization method would have been possibly more suitable. However, a successful optimization tool-chain was demonstrated using commercially available off-the-shelf software products.

ACKNOWLEDGMENT

The authors gratefully acknowledge support by the Deutsche Forschungsgemeinschaft (DFG) as part of collaborative research centre CRC 1029 ”Substantial efficiency increase in gas turbines through direct use of coupled unsteady combustion and flow dynamics”.

NOMENCLATURE

A	Area [m^2]
c	chordlength [m] / absolute velocity [$\mathrm{m/s}$]
f	camber line coordinate [m]
h	height [m] / enthalpy [$\mathrm{J/kg}$]
m'	arc length along a streamline in the meridian plane in the dim.less coordinate system [-]
n	number [-]
p	pressure [Pa]
r	radius/radial coordinate [m]
t	thickness [m]
u	tangential velocity of the blade [$\mathrm{m/s}$]
w	work [$\mathrm{J/kg}$]
x_f	maximum camber (camber reserve) [-]
x, y, z	cartesian coordinates (x corresponds to the rotor axis) [m]

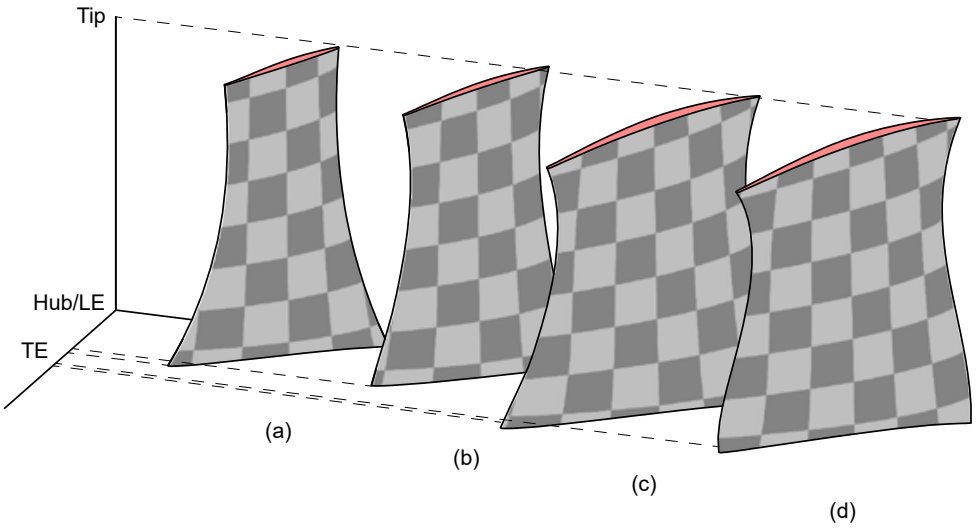

Fig. 14: DESIGN ITERATIONS OF THE ROTOR BLADE; (a) BASELINE DESIGN, (b) 2D MISES DESIGN, (c) 2D WIDE-CHORD MISES OPTIMIZED DESIGN, (d) FINAL 3D ANSYS OPTIMIZED DESIGN

Symbols

α	absolute turning angle [°]
β	relative turning angle [°]
η	isentropic efficiency [-]
ϑ	camber angle [°]
θ	circumferential angle [°]
Δ	difference [-]
λ	stagger angle [°]
ω	total pressure loss coefficient [-]
Ω	angular velocity of the rotor [$^1/_s$]
ρ	density [$^{kg}/_{m^3}$]

Indices

ax	axial
$base$	baseline
C	Compressor
CH	choked DP
$comb$	combined
DP	design point
E	Euler
i	inner
inf	infinity
mod	modification
o	outer
rel	relative
ST	stalled DP
s	specific
t	total
1	inlet
2	outlet

Abbreviations

2D	two dimensional
3D	three dimensional
CFD	computational fluid dynamics
DoE	design of experiments
DP	design point
LE	leading edge
PGC	pressure gain combustion
RANS	*Reynolds*-averaged *Navier–Stokes* equations
Se	Section
TE	trailing edge
VIGV	variable inlet guide vane

REFERENCES

[1] Deutsche Forschungsgemeinschaft (DFG), 2012. Collaborative research center 1029: Substantial efficiency increase in gas turbines through direct use of coupled unsteady combustion and flow dynamics. Retrieved September 20, 2019, from URL: `https://www.dfg.de/en/funded_projects/current_projects_programmes/list/projectdetails/index.jsp?id=200291049`.

[2] Brück, C., Tiedemann, C., and Peitsch, D., 2016. "Experimental investigations on highly loaded compressor airfoils with active flow control under non-steady flow conditions in a 3d-annular low-speed cascade". In Proceedings of the ASME Turbo Expo: Turbine Technical Conference and Exposition - 2016, The American Society of Mechanical Engineers, p. V02AT37A027.

[3] Brück, C., Mihalyovics, J., and Peitsch, D., 2018. "Experimental investigations on highly loaded compressor airfoils with different active flow control parameters under unsteady flow conditions". In Proceedings of the Global Power and Propulsion Society - North America Conference 2018, Global Power and Propulsion Society.

[4] Mihalyovics, J., Brück, C., Peitsch, D., Vasilopoulos, I., and Meyer, M., 2018. "Numerical and experi-

mental investigations on optimized 3d compressor airfoils". In Proceedings of the ASME Turbo Expo: Turbomachinery Technical Conference and Exposition - 2018, The American Society of Mechanical Engineers, p. V02AT39A038.

[5] Giannakoglou, K. C., Karakasis, M. K., and Kampolis, I. C., 2006. "Evolutionary algorithms with surrogate modeling for computationally expensive optimization problems". In Proceedings of ERCOFTAC 2006 Design Optimization International Conference, Gran Canaria, Spain.

[6] Yamazaki, W., and Mavriplis, D. J., 2013. "Derivative-enhanced variable fidelity surrogate modeling for aerodynamic functions". *AIAA Journal,* ***51***(1), pp. 126–137.

[7] Giles, M. B., and Pierce, N. A., 2000. "An introduction to the adjoint approach to design". *Flow, Turbulence and Combustion,* ***65***(3/4), pp. 393–415.

[8] Giles, M. B., Duta, M. C., Müller, J.-D., and Pierce, N. A., 2003. "Algorithm developments for discrete adjoint methods". *AIAA Journal,* ***41***(2), pp. 198–205.

[9] Papadimitriou, D. I., and Giannakoglou, K. C., 2006. "Compressor blade optimization using a continuous adjoint formulation". In Volume 6: Turbomachinery, Parts A and B, ASME, pp. 1309–1317.

[10] Cumpsty, N. A., 2004. *Compressor aerodynamics*, reprint edition 2004 w/new preface, introduction and updated bibliography ed. Krieger Publishing Company, Malabar, Florida.

[11] Aungier, R. H., 2003. *Axial-flow compressors: A strategy for aerodynamic design and analysis*. American Society of Mechanical Engineers, New York, N.Y. (ASME, Three Park Avenue. New York, NY 10016).

[12] Grieb, H., 2009. *Verdichter für Turbo-Flugtriebwerke*. Springer Berlin Heidelberg, Berlin, Heidelberg.